THE JOURNAL OF PHYSICAL CHEMISTRY B

Article

pubs.acs.org/JPCB

Ibuprofen and Propofol Cobinding Effect on Human Serum Albumin Unfolding in Urea

Alessandra Del Giudice, Claudia Leggio, Nicole Balasco,† Luciano Galantini, and Nicolae V. Pavel*

Dipartimento di Chimica, Sapienza Università di Roma, P.O. Box 34-Roma 62, Piazzale A. Moro 5, I-00185 Roma, Italy

Supporting Information

ABSTRACT: The unfolding pathway of the defatted human serum albumin (HSA) binding ibuprofen and propofol has been studied by using small-angle X-ray scattering (SAXS) and the support of circular dichroism data. A set of HSA solutions with urea concentrations between 0.00 and 9.00 M was analyzed, and the singular value decomposition method applied to the complete SAXS data set allowed us to distinguish four different states in solution. Besides the native and unfolded forms, two intermediates I1 and I2 have been identified, and the low-resolution structures of these states were obtained by exploiting both ab initio and rigid body fitting methods. The I1 structure was characterized by only one open domain (domain I, which does not host a binding site for either of the ligands), whereas I2 presents only one closed domain (domain III). A direct comparison with the unfolding pathway of the HSA:Ibu complex (Galantini et al. *Biophys. Chem.* **2010**, *147*, 111−122) pointed out that the presence of propofol as a second ligand, located in subdomain IIIB, leads to the appearance of an intermediate with two closed domains (domains II and III), which are those that accommodate the ligands. Moreover, the equilibrium between I2 and the unfolded form is slightly shifted toward higher urea concentrations. These results suggest that the cobinding significantly hinders the unfolding process.

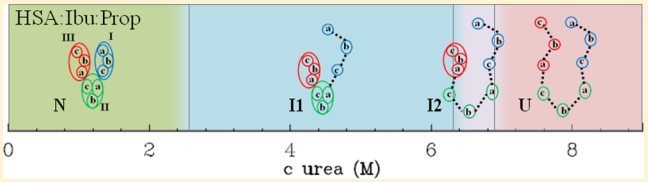

1. INTRODUCTION

Human serum albumin (HSA) is a monomeric, negatively charged protein with a molar mass of 66.5 kDa composed of 585 amino acids arranged in three homologous α-helical domains numbered I, II, and III, each divided into two subdomains, A and B.[1,2]

HSA is the most abundant plasma protein (with a typical concentration of 42 g/L in the bloodstream) having a prominent amount of physiological and pharmacological functions.[1,3−6] It is especially well known for its surprising ability to bind a large variety of endogenous and exogenous compounds, such as fatty acids, a huge variety of drugs, bile salts, hormones, and vitamins, in multiple sites. Albumin therefore acts as a primary carrier in human blood and has a crucial function in metabolism, distribution, and elimination of drugs. Its extraordinary transport ability ascribes to HSA both a protective action, by discharging different toxins, and an important antioxidant action, by entrapping ROS (reactive oxygen species), NO, and some chloride derivatives. Within the pharmacological applications, HSA, mainly as recombinant human albumin (rHSA), is widely used to extend the plasma half lives of therapeutic agents through reversible or covalent binding.[5,6] An excessively albumin high affinity for drugs is in some cases undesirable because it requires administration of higher doses. This effect is very important in the anesthetic pharmacology where the possibility of up to more than 50% of anesthetic binding to albumin must be considered in the administrations.[7]

In the light of the importance of the binding properties of HSA, much crystallographic and spectroscopic data on HSA:drug complexes has been reported in the literature,[7−11] and many efforts have been performed to correctly determine the number of binding sites.[12,13] Moreover, several studies in solution were focused on the stabilizing effect of ligand binding on the protein structure.[14−17] To highlight similar stabilizing effects, we recently reported a structural and spectroscopic combined study on the unfolding pathway of HSA binding ibuprofen (Ibu), a nonsteroidal anti-inflammatory drug.[18] As an extension of this study, in this work, the urea-induced unfolding of HSA in complex with two drugs is reported.

It is known that the investigation of the cobinding of different ligands with a target protein is particularly difficult due to the occurrence of effects such as competition for binding sites and cooperative or anticooperative phenomena.[19] In fact, several examples of mutual effects in the contemporary binding of different ligands have been pointed out for HSA, and the hypothesis that conformational protein changes are the main cause of these effects has been formulated.[17,20,21]

In this context, HSA started to be considered as an example of a monomeric protein with particular allosteric features.[22] These features, typical of a multimeric protein, seem to be evident also in the case of albumin because of its structural organization subdivided in domains hosting a variety of binding sites. Most of the albumin sites are dedicated to the binding of fatty acids; indeed, seven main sites of this kind have been located thanks to crystallographic data.[23,24] When HSA

Received: May 1, 2014
Revised: August 6, 2014
Published: August 8, 2014

dx.doi.org/10.1021/jp504280n | J. Phys. Chem. B 2014, 118, 10043−10051

accommodates the fatty acid molecules, slight conformational changes with relative motions between domains occur, and the structure becomes more stable in a denaturing process. As a matter of fact, thanks to the high association constants and the multiple binding sites, fatted HSA was reported to maintain its native structure up to a higher concentration of denaturant agents in comparison with the defatted HSA.[16]

Two of these fatty-acid hosting pockets are also high binding affinity regions for a variety of drugs: they are denoted as Sudlow's site I and II, located in subdomain IIA and IIIA, respectively.[25] Subdomain IB hosts another of these clefts, which is important, especially for being the heme binding site; it has been recognized as a quite flexible pocket because different molecules can bind in different arrangements inside this cavity,[26−28] and some experimental data has shown that the binding of ligands in this cleft often involves cooperativity or competition effects and allosteric coupling with contiguous sites.[8,9,20−22,29−32]

Information about competitive and concomitant influences of different ligands could be very important because some alterations in protein binding may alter the volume of distribution, clearance, and elimination of a drug and may modulate and modify its therapeutic effect.[20]

The anesthetic propofol (Prop) and the nonsteroidal anti-inflammatory drug Ibu were used as HSA-binding drugs in this work, and their effects on the urea-induced protein unfolding were reported. The complexes formed due to the binding of the single drug and the cobinding of both drugs were studied. The analysis was performed by circular dichroism (CD) on all systems. The denaturation-induced structural modification of the complex given by cobinding of both drugs was described by low-resolution structure analysis based on small-angle X-ray scattering (SAXS) data. The use of techniques that do not require the employment of probes[18,33−36] allowed us to avoid the presence of additional ligands that could bias the results of the measurements.

The crystallographic structure of HSA in complex with Prop has shown two binding sites. One molecule is hosted in subdomain IIIA, and the other binds in a cavity located in subdomain IIIB.[7]

Similarly, the high-resolution crystal structure of the HSA in complex with the anti-inflammatory drug Ibu has pointed out two binding sites: one in subdomain IIIA (the same of the Prop, named Sudlow's site II) and the other in a cleft at the interface between subdomains IIA and IIB.[8]

The induction or not of a greater protein stabilization due to the presence of either drugs Ibu and Prop with affinity for different binding sites could give us further information about the multistep unfolding mechanism of HSA, unveiling a possible influence of the cobinding on the stability of the different domains of the protein.

2. EXPERIMENTAL SECTION

2.1. Sample Preparation. HSA lyophilized powder, fatty acid, and globulin free (≥99%, type A3782), obtained from Sigma, was dissolved in 10 mM phosphate buffer at pH 7.4 with the addition of 11 mM sodium azide as preservative against molds and bacterial growth. The solution was filtered with a nucleopore filter with a diameter of 100 nm.

Ibu, type I4883, and Prop, type W505102, purchased from Sigma, were both dissolved in methanol of spectroscopic grade. These compounds were added, in a volume ∼40 μL, to the HSA defatted solution before the denaturant agent. Estimated methanol concentration in the HSA−drugs complex solutions was always <2% v/v.

After ∼5 h, the samples with urea, obtained from Riedel−Hahn, were prepared by adding a known volume of protein solution to the solid denaturant agent in volumetric flasks. After ∼10 h, the solutions were filtered again (diameter of 30 nm) and were analyzed in <1 week.

For the CD measurements, the HSA concentration was <1 g/L (15 μM). For the SAXS measurements, the protein concentration reached 4 g/L (60 μM). Protein concentration was determined spectrophotometrically using $\varepsilon_{280\ nm}$ = 35 700 M^{-1} cm^{-1}.[37] Bidistilled water was used in the preparation of the buffer. All experiments were conducted at room temperature (25 °C).

2.2. Spectroscopic Measurements. The absorbance measurements were performed with a Cary 1E UV−vis spectrophotometer. The CD spectra (four averaged acquisitions for far-UV experiments and 20 for near-UV) were recorded in a JASCO J-750 spectropolarimeter at 25 °C using a bandwidth of 1 nm. Path lengths of 0.1 mm and 1 cm were used, respectively, for the far-UV and near-UV spectra. The unfolding process was monitored by calculating the apparent folded fraction F_{app} considering in the far-UV the value of the mean residue ellipticity (MRE) at 222 nm (deg cm^2 $dmol^{-1}$), which increases linearly with the percentage of α helix[38] and the value of the MRE at 268 nm in the near-UV spectral range, where the CD spectrum shows a minimum.[10,39]

2.3. SAXS Measurements. In-house SAXS measurements were carried out in a thermostatically controlled (25.0 ± 0.1 °C) quartz capillary of 1 mm by using a Kratky compact camera, containing a slit collimation system, equipped with a NaI scintillation counter. Ni-filtered Cu Kα radiation (λ = 1.5418 Å) was used. Scattering curves were recorded within the range of $0.01 \leq q \leq 0.3$ $Å^{-1}$ ($q = 4\pi \sin(\theta)/\lambda$, where 2θ is the scattering angle). The moving slit method was employed to measure the intensity of the primary beam. The collimated scattering intensities were put on an absolute scale, subtracted for the solvent and the capillary contributions, and then expressed in electron units, eu (electrons^2 $Å^{-3}$) per centimeter primary-beam length.[40,41] In terms of total scattering cross section of an ensemble of particles, 1 eu corresponds to 7.94056×10^{-2} cm^{-1}.[42]

The indirect Fourier transform method developed in the ITP program was used for interpreting the spectra.[43] For very dilute samples (no particle interactions), the scattered intensity, $I(q)$, can be related to the pair distribution function $p(r)$ of the single scattering particle according to the equation

$$I(q) = \int_0^\infty p(r)\frac{\sin(qr)}{qr}\,dr$$

On the basis of this equation, the indirect Fourier transform method allows the extraction of the $p(r)$ function from the desmeared scattering pattern. The $p(r)$ function is strongly dependent on the shape and size of the scattering particles and vanishes at the maximum particle size, D_{max}. Furthermore, it permits an accurate determination of the electronic gyration radius, R_g.[43]

2.4. Singular Value Decomposition. We employed the singular value decomposition (SVD) method to determine the minimum number of structural states present in the HSA:Ibu:Prop 1:10:10 unfolding process. A detailed description of the procedure was previously reported.[16,18,44−46]

dx.doi.org/10.1021/jp504280n | J. Phys. Chem. B 2014, 118, 10043−10051

In brief, according to the SVD analysis, any scattering pattern in a set of curves at different urea concentrations can be approximated as the linear combination of a number of bases necessary to adequately reproduce the complete set of scattering intensities. In the SAXS data case, the $I(q)q^2$ functions are employed. Therefore, considering the presence of the native conformation in the absence of urea and of the unfolded form at urea 9.00 M, the analysis permitted us to draw the fraction of the structural states present at each urea concentration. The grid search step employed determined errors around 0.05 to 0.1 for the estimated fractions.

2.5. Three-Dimensional Reconstruction. Both an ab initio method (GA_STRUCT, supplied by W. T. Heller[47]) and a rigid-body modeling procedure (BUNCH[48]) were employed to find the probable 3D shape of the protein structural states involved in the unfolding by fitting their SAXS scattering patterns.

In the GA_STRUCT program, 50 starting models built from an aggregate of spheres related to the expected volume and the D_{max} of the scattering particle are improved using a genetic algorithm: the $p(r)$ of each model is calculated by means of a Monte Carlo method, and the fitness parameter is determined from the agreement between the calculated (Fourier transform) $I(q)$ and the experimental scattering pattern. Several runs of the minimization are automatically performed; at the end, all structures are checked for similarity. A consensus envelope is constructed from the model with the most common structural features, and 70% of the remaining models have the best overlap with it. The authors stress that the volume of the consensus envelope constitutes an index of the conformational flexibility: it is correlated with the spatial region ensemble occupied by most similar models. Therefore, its value will generally exceed the expected volume of a single frozen conformation in the case of a very flexible particle.[47,49]

In the BUNCH code, a hybrid approach using rigid-body fragments and flexible "dummy residue" linkers to model the polypeptide chain is implemented.[48] A simulated annealing protocol is used in the search procedure to fit the experimental data, and the basic rules of the conformational analysis are also fulfilled. For the rigid domains with known structure, the scattering patterns $I(q)$ are calculated with the code CRYSOL,[50] whereas the intensities corresponding to the portions represented as dummy residues are calculated using spherical harmonics.

In the case of HSA, starting from the crystallographic structure (PDB entry 2BXG) obtained from the Protein Data Bank,[8,51] the fragmentation was performed by dividing each HSA domain into three rigid moieties, taking into account the fact that the unfolding mechanism maintains intact the 17 disulfide bridges. In comparison with a polypeptide chain, the disulfide bridges drastically reduce the global protein flexibility.[52−55] The search for partially unfolded models can be carried out leaving free to expand rigid domains or fragments connected by flexible chains. More details are given in refs 16, 18, and 56. The calculations were repeated at least 10 times for each model. The similarity of the obtained structures was checked by using DAMAVER,[57] in which the superposition is performed by the SUPCOMB code.[58] The program gives a normalized spatial discrepancy (NSD) value that certifies the goodness of overlap and is used as a parameter to determine the difference between two 3D objects. NSDs for all possible pairs of models are computed, and the average NSDk for each structure is evaluated. The reconstruction with the lowest NSDk is selected as reference, and possible outliers with NSDk exceeding the global average ⟨NSD⟩+ 2Δ (NSD) are discarded.

To check the results consistency, we evaluated the agreement between the structures obtained with GA_STRUCT and BUNCH. For this purpose, the docking of the 3D ab initio envelope and rigid-body model was done with the program SUPCOMB.[58] From the calculated overlap goodness factor (NSD) and a visual inspection of the superposition, a comparison between the two shapes can be made.

The results obtained with the procedure of analysis previously presented were cross-checked with those obtained by the use of the program suite EOM (Ensemble Optimisation Method).[59,60] EOM allows us to quantitatively characterize intrinsically disordered or flexible proteins assuming a range of conformations in solution, which contribute to the SAXS pattern. From a randomly generated pool of conformers, an ensemble is selected to best fit the experimental SAXS curve. The optimized ensemble dimensional parameters (R_g and D_{max} of the conformers as well as average values) and the computed scattering intensity were compared with the experimental data.

3. RESULTS AND DISCUSSION

The far-UV CD spectra of solutions with HSA:Prop 1:10 and HSA:Ibu:Prop 1:10:10 were analyzed. The F_{app} functions obtained by the MRE_{222nm} values, with F_{app}= $MRE_{222nm}(t)$ − $MRE_{222nm}(9.00)/MRE_{222nm}(9.00)$ − $MRE_{222nm}(0.00)$ (where in brackets the urea molar concentration is reported), are shown in Figure 1 and compared with the data recently obtained for the HSA and HSA:Ibu 1:10 systems. (See ref 18.)

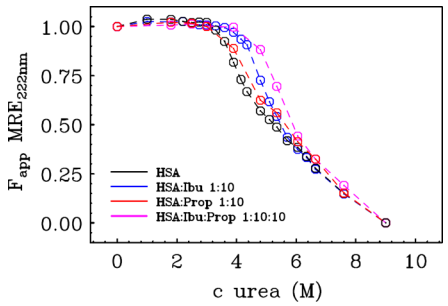

Figure 1. F_{app} calculated from the MRE at 222 nm at various urea concentrations for HSA with ibuprofen and propofol as ligands. For comparison, data of HSA and HSA:Ibu 1:10 systems (see ref 18) are shown.

By comparing the HSA:Ibu:Prop 1:10:10 system with the HSA:Ibu and HSA:Prop single drug complexes 1:10, the main result is that a marked stabilization is induced by the two cobound ligands. In particular, from 3.60 to 5.60 M urea, Prop presents a poor stabilizing efficiency. In the simultaneous presence of the two ligands, a higher percentage of α-helix is preserved up to ∼7.00 M urea.

Near-UV CD spectra of the HSA:Ibu:Prop 1:10:10 complex were also analyzed. CD in this spectral range is diagnostic of conformational changes affecting the tertiary structure because it reflects the structural rigidity that produces an asymmetrical environment around near-UV absorbing residues. The spectrum of the native form presents two minima with negative ellipticity at 261 and 268 nm and two shoulders at 279 and 283 nm. Variations of the two minima are especially attributed to perturbations around the many disulfide bridges, and the whole range is sensitive to conformational changes in the neighbor-

dx.doi.org/10.1021/jp504280n | J. Phys. Chem. B 2014, 118, 10043−10051

hood of the aromatic groups. (In particular, the signal between 290 and 300 nm can be attributed to the tryptophan.)[10,39]

As reported in Figure 2, a decrease in the ellipticity occurs by increasing urea concentration. From the corresponding

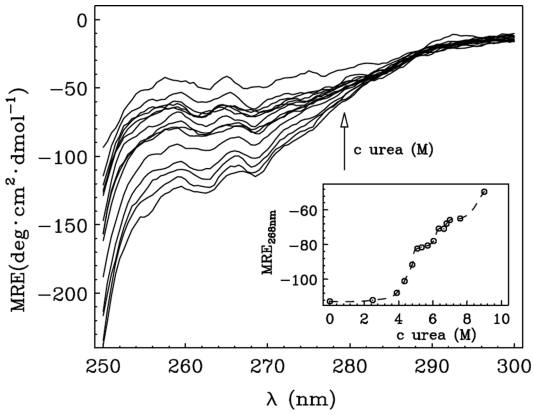

Figure 2. Near-UV CD spectra relative to HSA:Ibu:Prop solutions at increasing urea concentration (from 0.00 to 9.00 M; the arrow indicates the direction of the urea concentration increase). In the inset, the values of the MRE at 268 nm are reported as a function of urea molarity.

MRE_{268nm} values, we can see highlighted two steps around roughly 5.50 and 7.00 M urea (Figure 2 inset). A comparison with the complex HSA:Ibu 1:10 shows slightly lower values of ellipticity for the HSA:Ibu:Prop system in these two regions. This corresponds to slightly higher F_{app} values (Figure S1 in the Supporting Information) denoting a less pronounced variation of the tertiary structure for the latter system.

The differences between the two systems HSA:Ibu 1:10 and HSA:Ibu:Prop 1:10:10, observed with the CD technique, support the hypothesis that the albumin becomes more resistant to the chaotropic effect when the cavity located in subdomain IIIB is occupied by a site-specific ligand as Prop. We have therefore undertaken SAXS experiments on the HSA:Ibu:Prop 1:10:10 complex at different concentrations of urea to obtain structural information.

By applying the inverse Fourier transform, the SAXS spectra were interpreted, and dimensional parameters as R_g and D_{max} were determined together with the pair distribution functions $p(r)$. The agreement of the calculated intensities with the experimental ones and the corresponding $p(r)$ functions are shown in Figure S2 in the Supporting Information, while the R_g and D_{max} values are presented in Table S1 in the Supporting Information. An enhancement of the HSA stabilization because of the presence of Prop is evidenced in Figure 3 from a comparison between the R_g values of HSA binding the two drugs and of the HSA:Ibu 1:10 system. (See ref 18.) Indeed, for the complex with the two ligands, the R_g diagram shows a much slower growth by increasing the denaturant concentration up to 6.40 M, with R_g values sensitively lower than those of the HSA:Ibu samples in the urea concentration interval 4.40−6.40 M. A more detailed analysis of the trend shows a small jump of the R_g values around urea concentration of 3.00 M and a plateau in the range 3.00−6.00 M. A steep growth of the radius is caused by further increase in the denaturant concentration up to ∼8.00 M.

The evolution from a native to an unfolded state can be inferred from the shape of the $p(r)$ functions and from the $I(q)$ q^2 versus q plot, known as the Kratky plot (Figure 4). With the

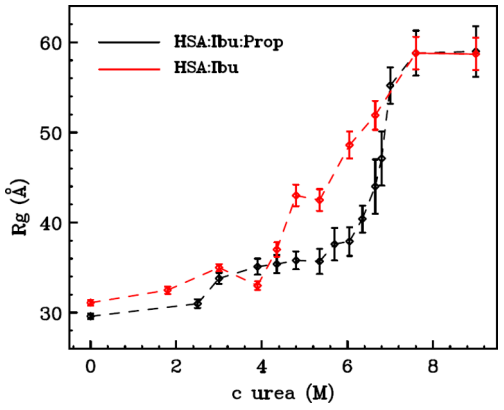

Figure 3. Gyration radii for HSA with ibuprofen and propofol as ligands at different urea concentrations. For comparison, data for HSA:Ibu 1:10 system (see ref 18) are shown.

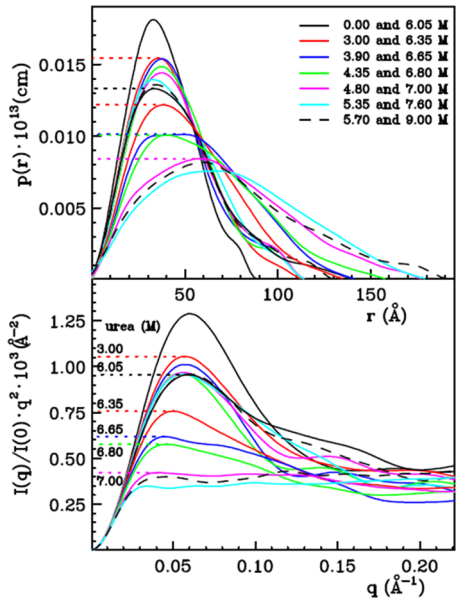

Figure 4. Pair distribution function $p(r)$ and Kratky plot of HSA:Ibu:Prop 1:10:10 at increasing urea concentration.

increase in the urea concentration, the D_{max} increases. Moreover, the Krakty plots gradually evolve from the typical bell-shaped profile of a native globular protein to the smooth curve characteristic of unfolded macromolecules. In agreement with the R_g pattern, the evolution of the $p(r)$ and Kratky plot show roughly invariant profiles in the range of denaturant concentration 3.00−6.00 M (see the plateau region of the R_g values in Figure 3), whereas a marked variation, supported by the R_g steep growth region in Figure 3, can be observed between 6.05 and 6.65 M of urea.

The minimum number of structural states present in the unfolding pathway has been determined by employing the SVD method for the analysis of the $I(q)q^2$ SAXS profiles. In addition to the native and unfolded forms, two intermediate states had to be taken into account (one state more than in the case of the HSA:Ibu 1:10 system[18]). By performing the study on the complete set of solutions, it was possible to obtain the values of the fractional populations of the native conformation $f_N(t)$, the two intermediates $f_{I1}(t)$ and $f_{I2}(t)$, and the unfolded form $f_U(t)$ at each urea concentration (t). The fractions of the four conformers are shown in Figure 5, and the values are reported

dx.doi.org/10.1021/jp504280n | J. Phys. Chem. B 2014, 118, 10043−10051

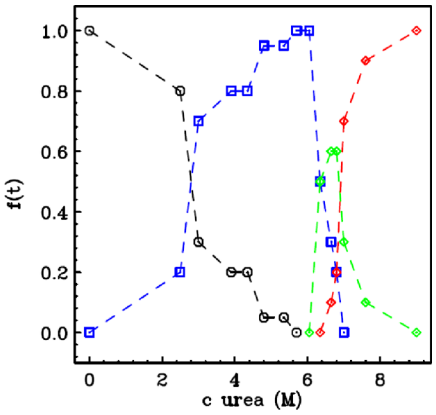

Figure 5. Fractional populations $f_N(t)$ (black), $f_{I1}(t)$ (blue), $f_{I2}(t)$ (green), and $f_U(t)$ (red) estimated by the SVD analysis of the $I(q)q^2$ SAXS profiles for the HSA:Ibu:Prop complex at all urea concentrations. $f(t)$ values have an absolute error of ~0.1.

in Table S2 in the Supporting Information. The intermediate I1 is dominant in a wide range of concentration of urea between 3.00 and 6.00 M. A second intermediate I2 is present at higher urea concentration in a narrow range. It reaches a maximum fraction of 0.6 and drops quickly in favor of the unfolded state. The f_{I1} and f_{I2} maxima are located in the same two regions of urea concentration, where the MRE_{268nm} plot presents the two steps (Figure 2). A comparison of the $p(r)$ functions allows us to suppose that this second intermediate could be to some extent similar to the one found in the HSA:Ibu system (Figure S3 in the Supporting Information).

The SVD analysis also provided the $I_{I1}(q)$ and $I_{I2}(q)$ scattering patterns of the two intermediates from which the $p(r)$ functions shown in Figures S3 and S4 in the Supporting Information were calculated. Corresponding gyration radii of 37 ± 1 Å ($R_{g,I1}$) and 45 ± 2 Å ($R_{g,I2}$), namely, between those of the native ($R_{g,N}$ = 29.5 ± 0.3 Å) and unfolded ($R_{g,U}$ = 59 ± 2 Å) forms, were extracted. The program GNOM[61] was used for the indirect Fourier inversion of the calculated scattering curve of the intermediate $I_2(q)$. Both the radii and scattering patterns of all conformers were used to estimate fraction weighted average gyration radii and $I(q)q^2$ functions for each urea concentration. Although affected by a significant uncertainty, mainly caused by propagated errors on the fractions (see Experimental Section), the experimental and the calculated values, shown in Figures 6 and 7, turned out to be very similar.

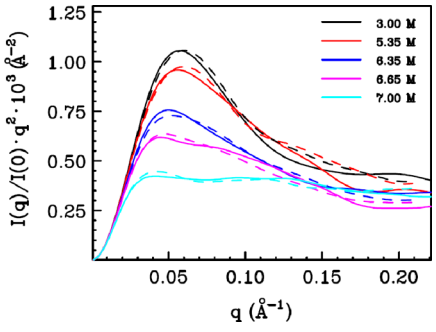

Figure 6. Kratky plots calculated by using the estimated fractions of conformers (dashed lines) compared with the experimental plots (continue lines) for urea concentrations where the two intermediates were mainly found.

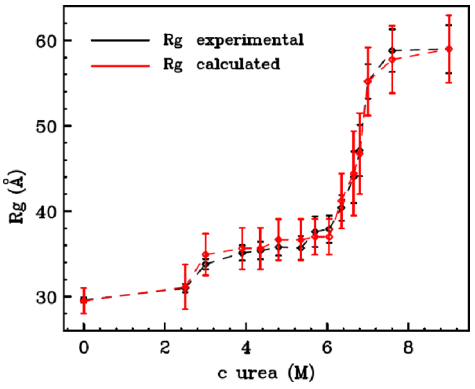

Figure 7. Comparison between the experimental gyration radii and those calculated by means of the estimated conformers fractions, for the HSA:Ibu:Prop complex at increasing urea concentration. The corresponding values are reported in Table S2 in the Supporting Information.

In this context, it is worthwhile noticing that for an SVD analysis performed with three bases only the agreement between the calculated and the experimental parameters is unsatisfactory.

In the recent past, the $I(q)$ patterns obtained from the SVD analysis allowed us to recover the low-resolution 3D structures for native, intermediates, and unfolded states present on the denaturation path in urea of HSA, HSA:palmitic acid, and HSA:Ibu.[16,18] A similar analysis has been undertaken in the present work. The 3D structures of the two intermediates involved in the unfolding pathway of the HSA:Ibu:Prop complex calculated with BUNCH are reported in Figure 8. For these two albumin conformers, recovered structures obtained with the GA_STRUCT program are also drawn together with their superimposition with the BUNCH structures.

For the intermediate I1, two spectra of the complex with urea 5.70 and 6.05 M have been contemporarily used. BUNCH minimizations have been performed for three possible models presenting one domain open: for each model, one of the three domains was left free to expand in three fragments connected by flexible linkers. At least 10 minimizations have been performed for each model. The analysis of the discrepancy $<\chi^2>$ values together with their estimated standard deviation (esd) values showed that the best agreement corresponds to the model with the domain I open. The minimizations performed by keeping open the domain II or the domain III give rise to calculated patterns with worse agreement indexes, namely, 1.35 and 1.15 times higher, respectively. The value 1.15 is not far, but the model can be still discarded because among the three domains, in the HSA:Ibu:Prop complex, domain I does not host any of the two ligands, and, in accordance with previous results also, it can be expected to be less stabilized.[16,18] All solutions obtained for the selected model (domain I open) by BUNCH and subsequently subjected to the superposition analysis passed the test of the NSD consistency with DAMAVER. The ⟨NSD⟩ and Δ(NSD) values are 1.32 and 0.11, respectively, whereas NSDk = 1.185 for the most similar model. This represents a further confirmation of the strict similarity among the BUNCH structures and the reliability of the proposed conformation. The structure with the lowest NSDk value was selected as the best description of the conformer. An inspection of this structure shows that the two closed domains (II and III) remain adjacent, although the

dx.doi.org/10.1021/jp504280n | J. Phys. Chem. B 2014, 118, 10043−10051

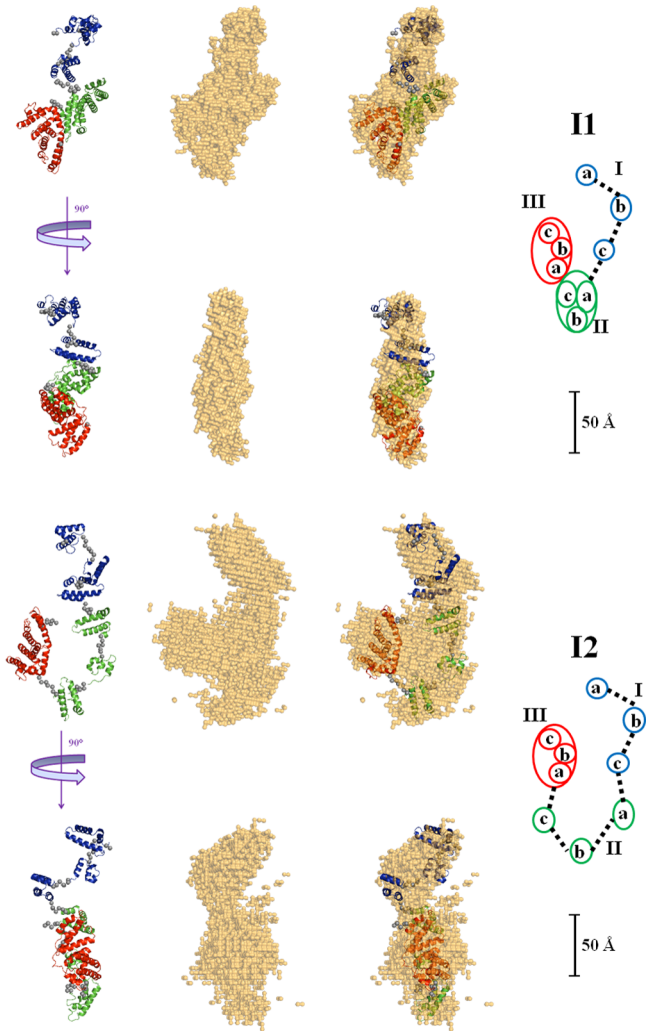

Figure 8. 3D structures of the two intermediates that evolve in solution in the urea-induced unfolding of the HSA:Ibu:Prop complex recovered from SAXS data. The structures obtained with the BUNCH code, GA_STRUCT consensus envelopes, and their superimpositions are shown. The three HSA I, II, and III domains are in blue, green, and red, respectively, while dummy residues are represented as gray spheres. Two orthogonal viewpoints are reported. On the right, a schematization of the relative opening of the domains is presented. This drawing has been built using PyMOL. The PyMOL Molecular Graphics System, version 1.5.0.4 is a trademark of Schrödinger.

distance between them (38 Å) is slightly greater than that found in the crystallographic structure (35 Å). The complementary ab initio reconstruction by GA_STRUCT provided a consensus envelope corresponding to R_g = 38 Å and D_{max} = 135 Å. The superposition between this envelope and the BUNCH proposed structure can be considered satisfactory. (See Figure 8.) According to an unfolding pathway of progressive opening of different domains, for the rigid body modeling undertaken to determine the structure of the second intermediate I2, we started from models with one domain (II or III) closed. This assumption is supported by the similarity of the R_g and D_{max} values obtained for this intermediate with those found for the HSA and HSA:Ibu intermediates[16,18] presenting two domains open. The agreements found for the two situations are quite similar, which is reasonable and is attributable to the increased flexibility that the protein acquires. The models obtained from repeated calculations show a better superimposition for the domain III closed, the ⟨NSD⟩ value being 1.17 ± 0.20 against 1.91 ± 0.35 obtained for the calculations performed keeping domain II closed. In favor of an intermediate with domain III closed, we can also invoke that the same type of conformation was found in the unfolding process of the HSA without ligands and HSA with Ibu. From calculations performed with GA_STRUCT program, similar envelopes (⟨NSD⟩ = 1.31) are obtained. The most representative was superimposed to all models obtained with BUNCH, where one domain (II or III) was kept closed. An inspection of the single NSDs as well as the ⟨NSD⟩ values is in favor of the intermediate that presents the domain III closed. The most representative rigid-body recovered structure, with a D_{max} = 152 Å in agreement with the value obtained from inverse Fourier transform, together with the envelope and their superposition are shown in Figure 8.

An attempt to model the scattering patterns of HSA:Ibu:-Prop at increasing urea concentration using the EOM program suite has also been made. Unfortunately, the results have pointed out that the application of this method on a multidomain protein under denaturation conditions fails to satisfactorily reproduce the experimental parameters (R_g, D_{max}) and the SAXS patterns in the whole range of urea concentration, leading to very large deviations at high denaturant molarity. For a good understanding of the results obtained with EOM, the details are presented as Supporting Information. In Figures S5 and S6 in the Supporting Information, the EOM R_g values and D_{max} values are shown and compared with the results previously presented; in Figure S7 in the Supporting Information, the EOM-selected R_g distributions are presented as a function of urea concentration, and in Figure S8 in the Supporting Information the residuals between experimental SAXS data and EOM best fits are shown.

EOM and the alternative minimal ensemble search (MES) method[62] give good results when flexible proteins are studied in water. Urea interacts strongly with the biopolymer chain, and the extended configurations are significantly more populated than in water, whereas protecting osmolytes favor less extended conformers.[63] Therefore, a quantitative description of denaturated state ensembles seems to be different compared with the water solution. Bernadò and Svergun recently asserted that EOM does not give good results on intrinsically disordered proteins when a denaturing agent is employed.[64] Conformational sampling in a chemically denatured state is not equivalent to that found for intrinsically disordered proteins under native conditions. In this regard, they discussed the results presented by Bernadò and Blackledge,[65] where "a 15% increase in extended conformations was required to describe R_g data measured for chemically denatured proteins".

This is in agreement with our EOM results at higher urea concentration, where the selected conformations are less extended than experimental parameters as R_g and D_{max} suggest. Bernadò and Blackledge achieved good results for chemically denatured proteins using not the standard coil database but a modified one, where "the overall population of extended conformations was systematically increased for each amino-acid-specific population".[65]

4. CONCLUSIONS

In summary, we found that in the urea-induced unfolding of the complex HSA:Ibu:Prop, a cooperative antidenaturing effect is observed due to the simultaneous presence of the two drugs, thus accounting for an increased stability of the HSA.

dx.doi.org/10.1021/jp504280n | J. Phys. Chem. B 2014, 118, 10043−10051

Compared with the information provided by the CD spectroscopy, the SAXS technique proved to be more diagnostic. The results pointed out that the complex unfolds sequentially with domain II opening after domain I, giving rise to two different intermediates, according to a pathway that is outlined and compared with that of HSA and HSA:Ibu complex in Figure 9.

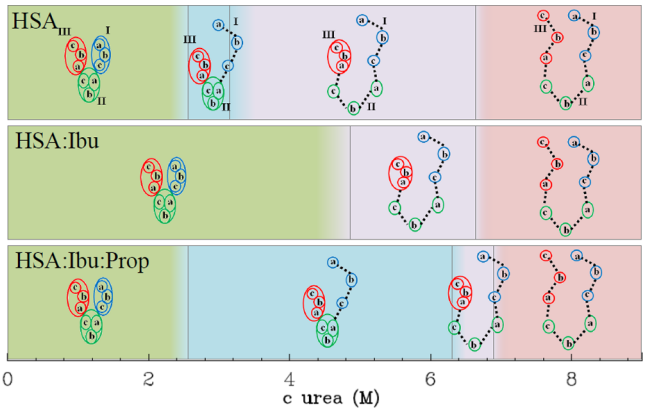

Figure 9. Comparison between the unfolding paths of the three systems HSA, HSA:Ibu, HSA:Ibu:Prop. The different-colored rectangles delimit the urea concentration intervals within which the presence of one of the HSA isomers prevails (≥50% ± 5%).

In the case of the ternary complex, the opening sequence is similar to that observed for HSA defatted, but on the scale of urea concentration, the intermediate I1 is stable up to a higher amount of denaturant at the expense of the second intermediate appearance.

Astonishingly, the denaturation pathway is significantly different compared with the unfolding of HSA:Ibu, where the formation of one intermediate only, with both domains I and II open, was sufficient to interpret the whole set of SAXS data. On the basis of crystallographic structures of the HSA:drug complexes, Ibu and Prop are expected to bind in the sites located within subdomains IIIB (Prop) and IIIA (both Ibu and Prop would compete for binding to this site) and at the interface between subdomains IIA and IIB (Ibu). Binding in another domain can be discarded at the drug:HSA ratios studied in this work,[8,9] although it has been reported in the literature for samples at very high ratios.[32]

The stabilizing effect on domain III of the two drugs is in agreement with the expected effect of direct binding to specific sites. This domain is also the most stable in the unfolding of pure HSA[16] and, from the evaluation of the models calculated by fitting SAXS data, it seems to be the most resistant to unfolding in our ternary complex as well.

The reported results suggest that the binding of Prop in addition to Ibu determines a destabilization of domain I, whereas it stabilizes domain II. Because the crystallographic structure shows that none of these domains are directly involved in binding Prop, a complex effect may be invoked to explain these results. Because of this effect, the Prop and Ibu cobinding make domains II and III more compact, whereas it weakens the contacts with domain I.

■ ASSOCIATED CONTENT

Supporting Information

Figure S1: F_{app} calculated from the MRE at 268 nm at increasing urea concentration for HSA:Ibu:Prop and comparison with HSA:Ibu. Figure S2: SAXS data and indirect Fourier inversion results. Table S1: Dimensional parameters obtained by SAXS data. Table S2: Isomer fractions and calculated R_g values corresponding to HSA:Ibu:Prop at different urea concentrations. Figure S3: Comparison between $p(r)$ functions of I2 and Iibu. Figure S4: Scattering patterns and $p(r)$ functions of the intermediates. Figure S5: R_g values and weight of the EOM selected conformers. Figure S6: D_{max} values and weight of the EOM selected conformers. Figure S7: R_g distributions obtained with EOM in the range 0−6.35 M as a function of urea concentration. Figure S8: Relative residuals for EOM and BUNCH fit results. This material is available free of charge via the Internet at http://pubs.acs.org.

■ AUTHOR INFORMATION

Corresponding Author

*E-mail: nicolaeviorel.pavel@uniroma1.it.

Present Address

†N.B.: Institute of Biostructures and Bioimaging, CNR, Via Mezzocannone 16, 80134 Naples, Italy and Second University of Naples, 81100 Caserta, Italy.

Author Contributions

The manuscript was written through contributions of all authors. All authors have given approval to the final version of the manuscript,

Notes

The authors declare no competing financial interest.

■ ACKNOWLEDGMENTS

Financial support from Sapienza University of Rome (Project C26A139RPZ) and CASPUR for the Standard HPC Grant 2009 Std09-408 is gratefully acknowledged. The technical assistance of Mr. Antonio Ulisse was very appreciated.

■ ABBREVIATIONS

HSA, human serum albumin; Ibu, ibuprofen; Prop, propofol; SAXS, small-angle X-ray scattering; CD, circular dichroism; MRE, mean residue ellipticity; SVD, singular value decomposition; NSD, normalized spatial discrepancy; rHSA, recombinant human serum albumin; ROS, reactive oxygen species; EOM, ensemble optimisation method; MES, minimal ensemble search; esd, estimated standard deviation

■ REFERENCES

(1) Peters, T., Jr. *All about Albumin: Biochemistry, Genetics and Medical Applications*; Academic Press: San Diego, CA, 2003; Chapter 2.

(2) Carter, D. C.; Ho, J. X. Structure of Serum Albumin. *Adv. Protein Chem.* **1994**, *45*, 153−203.

(3) Figge, J.; Rossing, T. H.; Fencl, V. The Role of Serum Proteins in Acid-Base Equilibria. *J. Lab. Clin. Med.* **1991**, *117*, 453−467.

(4) Anraku, M.; Chuang, V. T. G.; Maruyama, T.; Otagiri, M. Redox Properties of Serum Albumin. *Biochim. Biophys. Acta, Gen. Subj.* **2013**, *1830*, 5465−5472.

(5) Sleep, D.; Cameron, J.; Evans, L. R. Albumin as a Versatile Platform for Drug Half-Life Extension. *Biochim. Biophys. Acta, Gen. Subj.* **2013**, *1830*, 5526−5534.

(6) Chuang, V. T. G.; Kragh-Hansen, U.; Otagiri, M. Pharmaceutical Strategies Utilizing Recombinant Human Serum Albumin. *Pharm. Res.* **2002**, *19*, 569−577.
(7) Bhattacharya, A. A.; Curry, S.; Franks, N. P. Binding of the General Anesthetics Propofol and Halothane to Human Serum Albumin. High Resolution Crystal Structures. *J. Biol. Chem.* **2000**, *275*, 38731−38738.
(8) Ghuman, J.; Zunszain, P. A.; Petipas, I.; Bhattacharya, A. A.; Otagiri, M.; Curry, S. Structural Basis of the Drug-Binding Specificity of Human Serum Albumin. *J. Mol. Biol.* **2005**, *353*, 38−52.
(9) Zsila, F. Subdomain IB Is the Third Major Drug Binding Region of Human Serum Albumin: Toward the Three-Sites Model. *Mol. Pharmaceutics* **2013**, *10*, 1668−1682.
(10) Zsila, F. Circular Dichroism Spectroscopic Detection of Ligand Binding Induced Subdomain IB Specific Structural Adjustment of Human Serum Albumin. *J. Phys. Chem. B* **2013**, *117*, 10798−10806.
(11) Encinas, M. V.; Lissi, E.; Vergara, C. Association of Valdecoxib, a Nonsteroidal Anti-Inflammatory Drug, with Human Serum Albumin. *Photochem. Photobiol.* **2013**, *89*, 1399−1405.
(12) Zsila, F.; Bikadi, Z.; Malik, D.; Hari, P.; Pechan, I.; Berces, A.; Hazai, E. Evaluation of Drug−Human Serum Albumin Binding Interactions with Support Vector Machine Aided Online Automated Docking. *Bioinformatics* **2011**, *27*, 1806−1813.
(13) Lissi, E.; Calderon, C.; Campos, A. Evaluation of the Number of Binding Sites in Proteins from their Intrinsic Fluorescence: Limitations and Pitfalls. *Photochem. Photobiol.* **2013**, *89*, 1413−1416.
(14) Saso, L.; Valentini, G.; Casini, M. L.; Mattei, E.; Braghiroli, L.; Mazzanti, G.; Panzironi, C.; Grippa, E.; Silvestrini, B. Inhibition of Protein Denaturation by Fatty Acids, Bile Salts and Other Natural Substances: a New Hypothesis for the Mechanism of Action of Fish Oil in Rheumatic Diseases. *Jpn. J. Pharmacol.* **1999**, *79*, 89−99.
(15) Fanali, G.; Ascenzi, P.; Fasano, M. Effect of Prototypic Drugs Ibuprofen and Warfarin on Global Chaotropic Unfolding of Uuman Serum Heme−Albumin: a Fast-Field Cycling 1H NMR Relaxometric Study. *Biophys. Chem.* **2007**, *129*, 29−35.
(16) Leggio, C.; Galantini, L.; Konarev, P. V.; Pavel, N. V. Urea-Induced Denaturation Process on Defatted Human Serum Albumin and in the Presence of Palmitic Acid. *J. Phys. Chem. B* **2009**, *113*, 12590−12602.
(17) Varshney, A.; Ahmad, B.; Khan, R. H. Comparative Studies of Unfolding and Binding of Ligands to Human Serum Albumin in the Presence of Fatty Acid: Spectroscopic Approach. *Int. J. Biol. Macromol.* **2008**, *42*, 483−490.
(18) Galantini, L.; Leggio, C.; Konarev, P. V.; Pavel, N. V. Human Serum Albumin Binding Ibuprofen: A 3D Description of the Unfolding Pathway in Urea. *Biophys. Chem.* **2010**, *147*, 111−122.
(19) Ascoli, G.; Bertucci, C.; Salvadori, P. Stereospecific and Competitive Binding of Drugs to Human Serum Albumin: a Difference Circular Dichroism Approach. *J. Pharm. Sci.* **1995**, *84*, 737−741.
(20) Varshney, A.; Sen, P.; Ahmad, E.; Rehan, M.; Subbarao, N.; Khan, R. H. Ligand Binding Strategies of Human Serum Albumin: How Can The Cargo be Utilized? *Chirality* **2010**, *22*, 77−87.
(21) Fanali, G.; di Masi, A.; Trezza, V.; Marino, M.; Fasano, M.; Ascenzi, P. Human Serum Albumin: From Bench to Bedside. *Mol. Aspects Med.* **2012**, *33*, 209−290.
(22) Ascenzi, P.; Fasano, M. Allostery in a Monomeric Protein: the Case of Human Serum Albumin. *Biophys. Chem.* **2010**, *148*, 16−22.
(23) Curry, S.; Mandelkow, H.; Brick, P.; Franks, N. Crystal Structure of Human Serum Albumin Complexed with Fatty Acid Reveals an Asymmetric Distribution of Binding Sites. *Nat. Struct. Biol.* **1998**, *5*, 827−835.
(24) Bhattacharya, A. A.; Grune, T.; Curry, S. Crystallographic Analysis Reveals Common Modes of Binding of Medium and Long-Chain Fatty Acids to Human Serum Albumin. *J. Mol. Biol.* **2000**, *303*, 721−732.
(25) Sudlow, G.; Birkett, D. J.; Wade, D. N. The Characterization of Two Specific Drug Binding Sites on Human Serum Albumin. *Mol. Pharmacol.* **1975**, *11*, 824−832.
(26) Curry, S. Lessons from the Crystallographic Analysis of Small Molecule Binding to Human Serum Albumin. *Drug Metab. Pharmacokinet.* **2009**, *24*, 342−357.
(27) Zunszain, P. A.; Ghuman, J.; McDonagh, A. F.; Curry, S. Crystallographic Analysis of Human Serum Albumin Complexed with 4Z, 15E-bilirubin-IXα. *J. Mol. Biol.* **2008**, *381*, 394−406.
(28) Zunszain, P. A.; Ghuman, J.; Komatsu, T.; Tsuchida, E.; Curry,S. Crystal Structural Analysis of Human Serum Albumin Complexed with Hemin and Fatty Acid. *BMC Struct. Biol.* **2003**, *3*, No. 6.
(29) Ryan, A. J.; Ghuman, J.; Zunszain, P. A.; Chung, C. W.; Curry, S. Structural Basis of Binding of Fluorescent, Site-Specific Dansylated Amino Acids to Human Serum Albumin. *J. Struct. Biol.* **2011**, *174*, 84−91.
(30) Zhu, L.; Yang, F.; Chen, L.; Meehan, E. J.; Huang, M. A New Drug Binding Subsite on Human Serum Albumin and Drug−Drug Interaction Studied by X-Ray Crystallography. *J. Struct. Biol.* **2008**, *162*, 40−49.
(31) Nicoletti, F. P.; Howes, B. D.; Fittipaldi, M.; Fanali, G.; Fasano, M.; Ascenzi, P.; Smulevich, G. Ibuprofen Induces an Allosteric Conformational Transition in the Heme Complex of Human Serum Albumin with Significant Effects on Heme Ligation. *J. Am. Chem. Soc.* **2008**, *130*, 11677−11688.
(32) Ascenzi, P.; di Masi, A.; De Sanctis, G.; Coletta, M.; Fasano, M. Ibuprofen Modulates Allosterically NO Dissociation from Ferrous Nitrosylated Human Serum Heme-Albumin by Binding to Three Sites. *Biochem. Biophys. Res. Commun.* **2009**, *387*, 83−86.
(33) Tayyab, S.; Sharma, N.; Khan, M. M. Use of Domain Specific Ligands to Study Urea-Induced Unfolding of Bovine Serum Albumin. *Biochem. Biophys. Res. Commun.* **2000**, *277*, 83−88.
(34) Ahmad, B.; Khan, M. K. A.; Haq, S. K.; Khan, R. H. Intermediate Formation at Lower Urea Concentration in 'B' Isomer of Human Serum Albumin: a Case Study Using Domain Specific Ligands. *Biochem. Biophys. Res. Commun.* **2004**, *314*, 166−173.
(35) Santra, M. K.; Banerjee, A.; Krishnakumar, S. S.; Rahaman, O.; Panda, D. Multiple-Probe Analysis of Folding and Unfolding Pathways of Human Serum Albumin. Evidence for a Framework Mechanism of Folding. *Eur. J. Biochem.* **2004**, *271*, 1789−1797.
(36) Ahmad, B.; Ahmed, M. Z.; Haq, S. K.; Khan, R. H. Guanidine Hydrochloride Denaturation of Human Serum Albumin Originates by Local Unfolding of Some Stable Loops in Domain III. *Biochim. Biophys. Acta* **2005**, *1750*, 93−102.
(37) Pace, C. N.; Vajdos, F.; Fee, L.; Grimsley, G.; Gray, T. How to Measure and Predict the Molar Absorption Coefficient of a Protein. *Protein Sci.* **1995**, *4*, 2411−2423.
(38) Chen, Y. H.; Yang, J. T.; Martinez, H. M. Determination of the Secondary Structures of Proteins by Circular Dichroism and Optical Rotatory Dispersion. *Biochemistry* **1972**, *11*, 4120−4131.
(39) Dockal, M.; Carter, D.; Rüker, F. Conformational Transitions of the Three Recombinant Domains of Human Serum Albumin Depending on pH. *J. Biol. Chem.* **2000**, *275*, 3042−3050.
(40) Stabinger, H.; Kratky, O. A New Technique for the Measurement of the Absolute Intensity of X-Ray Small Angle Scattering, the Moving Slit Method. *Makromol. Chem.* **1978**, *179*, 1655−1659.
(41) Glatter, O. In *Small Angle X-ray Scattering*; Glatter, O., Kratky, O., Eds.; Academic Press: London, 1982; pp 119−165.
(42) Orthaber, D.; Bergmann, A.; Glatter, O. SAXS Experiments on Absolute Scale with Kratky Systems using Water as a Secondary Standard. *J. Appl. Crystallogr.* **2000**, *33*, 218−225.
(43) Glatter, O. A New Method for the Evaluation of Small-Angle Scattering Data. *J. Appl. Crystallogr.* **1977**, *10*, 415−421.
(44) Chen, L.; Hodgson, K. O.; Doniach, S. A Lysozyme Folding Intermediate Revealed by Solution X-ray Scattering. *J. Mol. Biol.* **1996**, *261*, 658−671.
(45) Segel, D. J.; Fink, A. L.; Hodgson, K. O.; Doniach, S. Protein Denaturation: A Small-Angle X-ray Scattering Study of the Ensemble of Unfolded States of Cytochrome *c*. *Biochemistry* **1998**, *37*, 12443−12451.

(46) Henry, E. R.; Hofrichter, J. Singular Value Decomposition: Application to Analysis of Experimental Data. *J. Methods Enzymol.* **1992**, *210*, 129−192.
(47) Heller, W. T.; Krueger, J. K.; Trewhella, J. Further Insights into Calmodulin-Myosin Light Chain Kinase Interaction from Solution Scattering and Shape Restoration. *Biochemistry* **2003**, *42*, 10579−10588.
(48) Petoukhov, M. V.; Svergun, D. I. Global Rigid Body Modeling of Macromolecular Complexes against Small-Angle Scattering Data. *Biophys. J.* **2005**, *89*, 1237−1250.
(49) Heller, W. T. Influence of Multiple Well Defined Conformations on Small-Angle Scattering of Proteins in Solution. *Acta Crystallogr., Sect. D* **2005**, *61*, 33−44.
(50) Svergun, D.; Barberato, C.; Koch, M. H. J. CRYSOL - A Program to Evaluate X-Ray Solution Scattering of Biological Macromolecules from Atomic Coordinates. *J. Appl. Crystallogr.* **1995**, *28*, 768−773.
(51) Bernstein, F. C.; Koetzle, T. F.; Williams, G. J.; Meyer, E. E., Jr.; Brice, M. D.; Rodgers, J. R.; Kennard, O.; Shimanouchi, T.; Tasumi, M. The Protein Data Bank: A Computer-based Archival File For Macromolecular Structures. *J. Mol. Biol.* **1977**, *112*, 535−542.
(52) Takeda, K.; Moriyama, Y. Comment on the Misunderstanding of the BSA−SDS Complex Model: Concern about Publications of an Impractical Model. *J. Phys. Chem. B* **2007**, *111*, 1244−1244.
(53) Leggio, C.; Galantini, L.; Pavel, N. V. About the Albumin Structure in Solution: Cigar Expanded form versus Heart Normal Shape. *Phys. Chem. Chem. Phys.* **2008**, *10*, 6741−6750.
(54) Castellanos, M. M.; Colina, C. M. Molecular Dynamics Simulations of Human Serum Albumin and Role of Disulfide Bonds. *J. Phys. Chem. B* **2013**, *117*, 11895−11905.
(55) Baler, K.; Martin, O. A.; Carignano, M. A.; Ameer, G. A.; Vila, J. A.; Szleifer, I. Electrostatic Unfolding and Interactions of Albumin Driven by pH Changes: A Molecular Dynamics Study. *J. Phys. Chem. B* **2014**, *118*, 921−930.
(56) Galantini, L.; Leggio, C.; Pavel, N. V. Human Serum Albumin Unfolding: A Small-Angle X-ray Scattering and Light Scattering Study. *J. Phys. Chem. B* **2008**, *112*, 15460−15469.
(57) Volkov, V. V.; Svergun, D. I. Uniqueness of Ab-Initio Shape Determination in Small-Angle Scattering. *J. Appl. Crystallogr.* **2003**, *36*, 860−864.
(58) Kozin, M.; Svergun, D. I. Automated Matching of High- and Low-Resolution Structural Models. *J. Appl. Crystallogr.* **2001**, *34*, 33−41.
(59) Bernadò, P.; Mylonas, E.; Petoukhov, M. V.; Blackledge, M.; Svergun, D. I. Structural Characterization of Flexible Proteins Using Small-Angle X-ray Scattering. *J. Am. Chem. Soc.* **2007**, *129*, 5656−5664.
(60) Petoukhov, M. V.; Franke, D.; Shkumatov, A. V.; Tria, G.; Kikhney, A. G.; Gajda, M.; Gorba, C.; Mertens, H. D. T.; Konarev, P. V.; Svergun, D. I. New Developments in the ATSAS Program Package for Small-Angle Scattering Data Analysis. *J. Appl. Crystallogr.* **2012**, *45*, 342−350.
(61) Svergun, D. I. Determination of the Regularization Parameter in Indirect-Transform Methods Using Perceptual Criteria. *J. Appl. Crystallogr.* **1992**, *25*, 495−503.
(62) Pelikan, M.; Hura, G. L.; Hammel, M. Structure and Flexibility within Proteins as Identified through Small Angle X-ray Scattering. *Gen. Physiol. Biophys.* **2009**, *28*, 174−189.
(63) Mondal, J.; Stirnemann, G.; Berne, B. J. When Does Trimethylamine N-Oxide Fold a Polymer Chain and Urea Unfold It? *J. Phys. Chem. B* **2013**, *117*, 8723−8732.
(64) Bernadò, P.; Svergun, D. I. Structural Analysis of Intrinsically Disordered Proteins by Small-Angle X-ray Scattering. *Mol. Biosyst.* **2012**, *8*, 151−167.
(65) Bernadò, P.; Blackledge, M. A Self-Consistent Description of the Conformational Behavior of Chemically Denatured Proteins from NMR and Small Angle Scattering. *Biophys. J.* **2009**, *97*, 2839−2845.